The laminar flow tube reactor as a quantitative tool for nucleation studies: Experimental results and theoretical analysis of homogeneous nucleation of dibutylphthalate

Vladimir B. Mikheev, Nels S. Laulainen, and Stephan E. Barlow
Pacific Northwest National Laboratory, Richland, Washington

Michael Knott and Ian J. Ford
Department of Physics and Astronomy, University College London, Gower Street, London WC1E 6BT, United Kingdom

(Received 24 March 2000; accepted 2 June 2000)

A laminar flow tube reactor was designed and constructed to provide an accurate, quantitative measurement of a nucleation rate as a function of supersaturation and temperature. Measurements of nucleation of a supersaturated vapor of dibutylphthalate have been made for the temperature range from −30.3 to +19.1 °C. A thorough analysis of the possible sources of experimental uncertainties (such as defining the correct value of the initial vapor concentration, temperature boundary conditions on the reactor walls, accuracy of the calculations of the thermodynamic parameters of the nucleation zone, and particle concentration measurement) is given. Both isothermal and the isobaric nucleation rates were measured. The experimental data obtained were compared with the measurements of other experimental groups and with theoretical predictions made on the basis of the self-consistency correction nucleation theory. Theoretical analysis, based on the first and the second nucleation theorems, is also presented. The critical cluster size and the excess of internal energy of the critical cluster are obtained. © *2000 American Institute of Physics.* [S0021-9606(00)51133-7]

I. INTRODUCTION

During the last few years definite progress has been achieved in both the theoretical and experimental aspects of nucleation. Many recently published papers have been devoted to the development of nucleation theory. Calculations of nucleation rates have been made using a variety of approaches and approximations. However, there is still great uncertainty concerning the estimation of the absolute value of the nucleation rate. The usual inadequacy of the classical thermodynamic approach appears every time when one approaches small cluster sizes, while modern calculations based on first principles, or the statistical mechanical approach, are hampered by uncertainties in how to represent a physical cluster.

Fortunately, there exist some theoretical results which are more secure. The derivative of the nucleation rate with respect to supersaturation is related to the size of the critical cluster, the size of which is equally likely to grow or to decay under the prevailing circumstances. This so-called first nucleation theorem[1–5] has been shown to be valid from several different points of view (including scaling considerations[4] and statistical ensemble arguments[5]), largely independent of the assumptions employed in the theory. Another important characteristic is the temperature dependence of the nucleation rate. The so-called second nucleation theorem[5–9] connects this dependence to the excess internal energy (loosely the surface energy) of the critical cluster.

With respect to experimental results, it should be noted that a shortage of valid quantitative experimental data still exists. In order to provide quantitative tests of nucleation theories, accurate and reliable nucleation rate measurements as functions of supersaturation and temperature are required. Although various experimental approaches have been developed for nucleation studies,[10] it must be noted that, since nucleation is extremely sensitive to any shift in supersaturation or temperature, the accuracy of defining these parameters sets very high requirements for the measurements that can be characterized as quantitative. In our opinion, among the various experimental techniques currently designed for nucleation studies, only two of them have been shown to provide such quantitative nucleation rate data. Expansion cloud chamber[11,12] and thermal diffusion cloud chamber[13,14] experimental measurements have been carried out for many years with increasing improvement of their level of accuracy and are the ''most commonly used for these types of nucleation measurements.'' [10]

Among the other experimental techniques, which are also contending to be in the category of quantitative tools, the expansion wave tube technique[15] can be mentioned. This experimental device (which exploits the expansion principle) has been under systematic development during the past several years.[16] The results obtained using this technique provide very interesting information for the high range of nucleation rate values and particularly for high total pressure conditions.

Another very promising tool for precise nucleation measurements is the laminar flow technique,[1,3,17–21] which applies the principle of the thermal diffusion chamber for the flow conditions. Today, this device attracts considerable at-

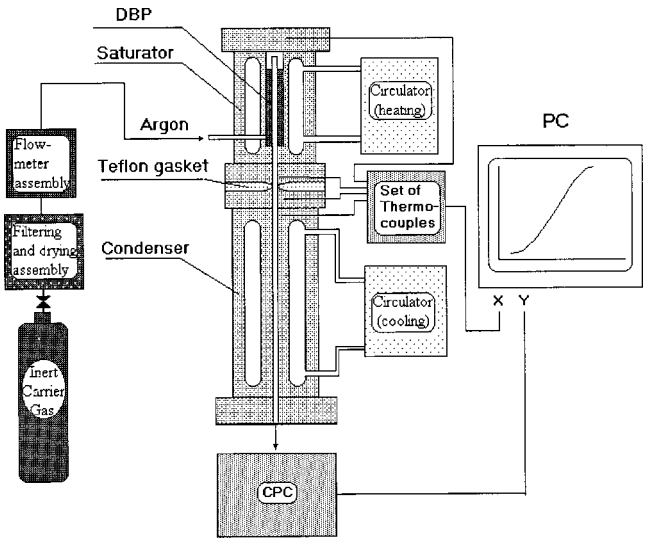

FIG. 1. General schematic of the experimental setup.

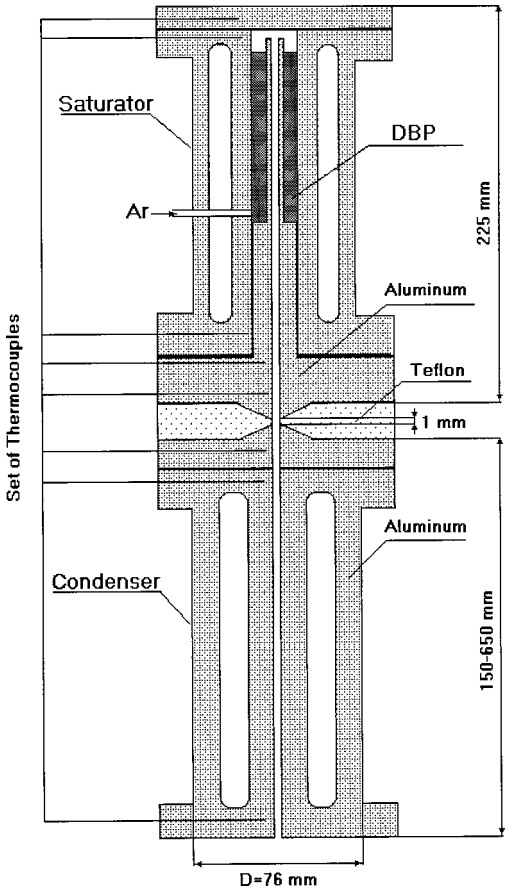

FIG. 2. Laminar flow tube reactor detail. Condenser consists of several identical sections so that the length of the condenser can be varied.

tention among investigators.[22,23] However, the current state of the measurement of nucleation of dibutylphthalate (DBP), which can be considered as a more-or-less traditional standard substance for the laminar flow technique, shows discrepancies between the data obtained by different groups of experimentalists.[3,17,20] This is not a surprise, because the process of nucleation is so difficult to measure that, as already noted above, dozens of years of experience have been required to verify both well-known expansion cloud chamber and the thermal diffusion chamber techniques. Consequently, we feel that a very thorough analysis of the laminar flow technique is essential to understand the reasons for possible experimental inaccuracies and uncertainties. This is one of the main objectives of this paper. The other is to present new experimental data for DBP. DBP has been used by various experimental groups for nucleation measurements by the laminar flow type technique.[3,17,20,21] Although we would like to extend our measurements, on one hand, to cover the different types of compounds which are of common interest to nucleation researchers (water, alkanes, alcohols, and particularly *n*-pentanol, which was chosen as a standard during the Workshop on Nucleation Experiments in Prague, June 1995), we believe it is urgently necessary to substantiate the validity of the laminar flow device, on the other, by focusing our attention on DBP.

II. EXPERIMENT

A. Principles of operation

The principle of operation of the LFTR (laminar flow tube reactor, or laminar flow diffusion chamber,[17] or flow diffusion nucleation chamber[18]) is relatively simple. Figure 1 represents the general schematic of the experimental device used in the study and is a useful reference diagram for the discussions that follow. Figure 2 provides additional details of the LFTR itself.

Typically, the LFTR consists of two thermally separated parts. A ''hot'' part, called the saturator, and a ''cold'' part, called the condenser. In our case, both saturator and condenser are made from aluminum cylinders of 76 mm external diameter. The total length of the saturator is 225 mm and the length of the condenser can be varied from 150 to 650 mm. The diameter of the internal channel is 8 mm. Both the saturator and condenser are constructed with jackets for liquid circulation to support the required temperatures. NESLAB RTE Refrigerated Circulators are used for temperature control and have a temperature stability of $\pm 0.05\,^{\circ}\mathrm{C}$. A Teflon® gasket (5 mm thick) serves for the thermo-insulation between saturator and condenser. However, because of the cone-shaped interior protrusion on both faces of the saturator and condenser, and consequently the concave cone shape for the Teflon® gasket, we have been able to attain a 1 mm thick insulation between the internal channels of the saturator and of the condenser. Several narrow (less than 1 mm diameter) wells have been drilled at different locations in both saturator and condenser to monitor the temperature. In addition, special temperature measurements directly inside the internal channel can be made. K-type thermocouples (0.25 mm diameter) are used for the temperature measurements.

The operation of the LFTR is as follows. First, an inert carrier gas (ultra-high purity argon, 99.999%) is injected into the saturator, where, while passing through a molecular sieve (1 mm grain diameter) impregnated by some substance of interest (in the present case, DBP at 99% purity), the carrier gas becomes saturated by the vapor of the substance at the temperature of the saturator. The vapor-gas flow then enters

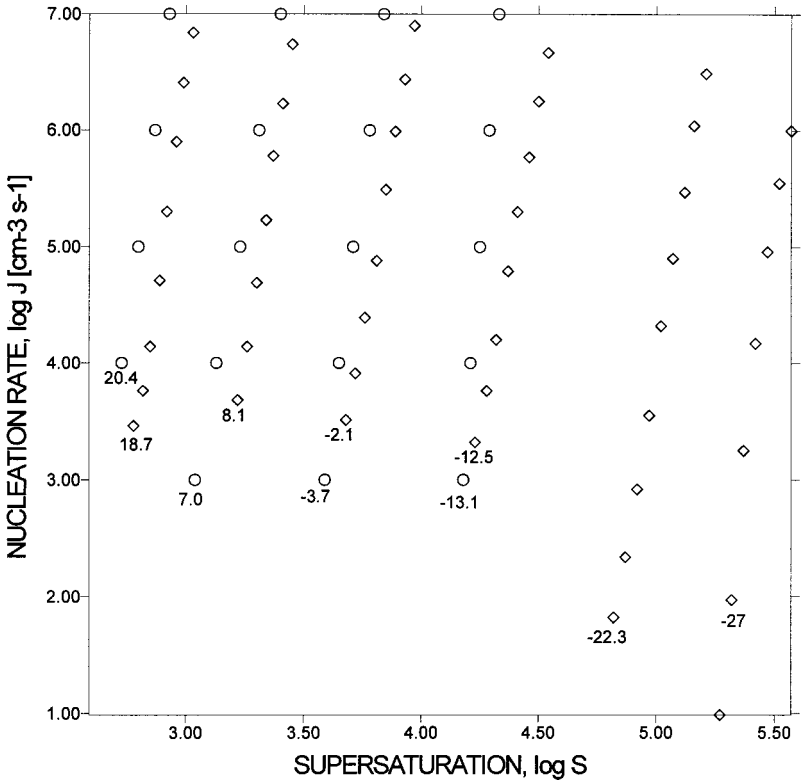

FIG. 3. Comparison of our previous experimental data (Ref. 17) obtained for the system DBP–Ar (circles) and the Hämeri *et al.* (Ref. 15) results obtained for the system DBP-N_2 (diamonds). The nucleation temperatures (C) are indicated at the lowest point of each data set.

the internal channel of the reactor and, after passing through the entire length of saturator section, it enters the internal channel of the condenser. Here, through the process of cooling, a supersaturated state is achieved and DBP particles begin to nucleate. Once the gas flow leaves the condenser, the concentration of the particles formed in the LFTR can be determined by an appropriate particle counter. We are currently using a condensation particle counter (CPC) (TSI-3025A), which is based on particle light scattering (typically after further enlargement in the CPC). The apparatus is operated at normal atmospheric pressure. The entire system is interfaced to a PC, so the particle concentration dependence upon the temperatures and flow rate can be plotted and recorded. The PC also serves to control the operation of the system.

Because the flow is laminar (volume flow rate is 5 cm^3/s and the diameter of the internal channel of the reactor is 8 mm), one can calculate the spatial distributions of temperature, vapor concentration, and supersaturation. Hence, the nucleation rate profile inside the internal channel of the reactor can be modeled using the known initial conditions (vapor concentration and temperature) of the flow at the inlet to the channel and also using the known boundary conditions on the walls of the channel (temperature and equilibrium vapor concentration). This allows us to define the nucleation zone, as well as to determine the nucleation volume and the residence time. (Self-consistent correction nucleation theory[25] has been applied for the modeling of nucleation rate profile, but, as shown by Hämeri *et al.*,[17] the determination of the nucleation zone does not depend upon the particular theory used.) From this information, the experimental value of the nucleation rate can be determined as a function of temperature, vapor concentration, and/or supersaturation (using the typical procedure described in details in Hämeri *et al.*[17]).

Such a simple construction and operation should give valid reproducible results, but in fact, as mentioned earlier, the comparison of the experimental data obtained by different groups of experimentalists[3,17,20] for the same substance (DBP) shows serious discrepancies (Figs. 3–5). In this paper we examine the potential weaknesses of this experimental technique to evaluate possible inaccuracies that may lead to the observed discrepancies. The following section provides a step-by-step analysis of possible sources of error.

B. Possible sources of error and uncertainty

1. Initial conditions for vapor pressure

The first question about accuracy arises immediately after the inert carrier gas enters the saturator. Is there sufficient residence time in the saturator for the inert gas to become completely saturated by the vapor of the substance under study? In other words, we need to make sure that the initial concentration at the inlet to the internal channel of the saturator in fact corresponds to the equilibrium vapor pressure of our substance at the temperature of saturator. This is not a trivial question. It is not easy to calculate the residence time for the internal geometry of the saturator used in our study and for the constructions used by other investigators.[3,17]

For a test experiment, we used a saturator that was a constant diameter (8 mm) straight tube and filled with a typically used molecular sieve (grain diameter 1 mm) impregnated by DBP. The length of the tube was 50 cm and the volume flow rate was 5 cm^3/s. For such a construction the residence time can be easily defined and is approximately 5 s. We tested this saturator and found that 5 s was insufficient

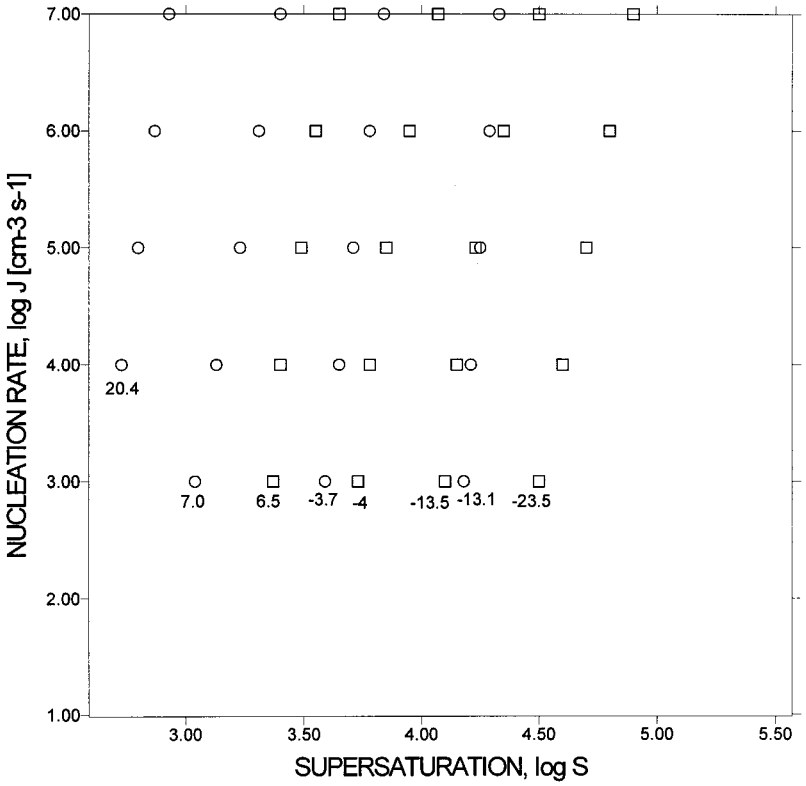

FIG. 4. Comparison of our previous experimental data (Ref. 17) obtained for the system DBP–Ar (circles) and the Bedanov *et al.* (Ref. 3) results obtained for the system DBP-N_2 (squares). The nucleation temperatures (C) are indicated at the lowest point of each data set.

for argon to be saturated by DBP vapor. However, Hämeri *et al.*[17] reported that the residence time in their saturator was less than 1 s and asserted that this was enough for saturation. We suggest that this value may not be correct and believe that the residence time in their saturator may be higher than their estimate. We found empirically that if the diameter of the internal column of the saturator is several times larger than the diameter of the outlet, then the inert gas has enough time to become saturated by the vapor of substance under study. Hämeri *et al.*[17] used exactly this kind of construction, but there is still a question of what the true residence time was.

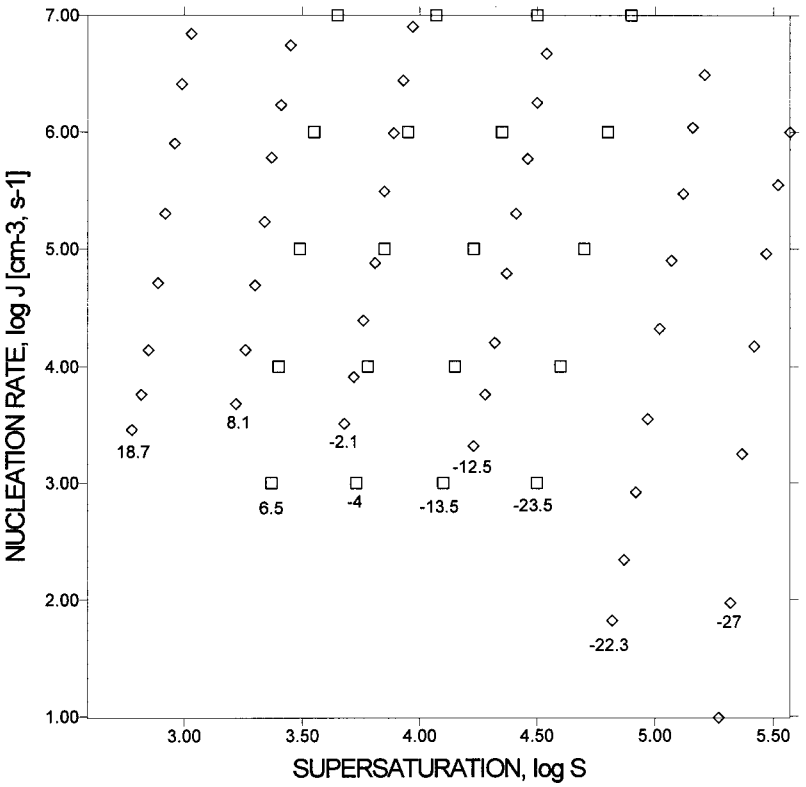

FIG. 5. Comparison of the Hämeri *et al.* (Ref. 15) experimental data obtained for the system DBP–N_2 (diamonds) and the Bedanov *et al.* (Ref. 3) results obtained for the system DBP–N_2 (squares). The nucleation temperatures (C) are indicated at the lowest point of each data set.

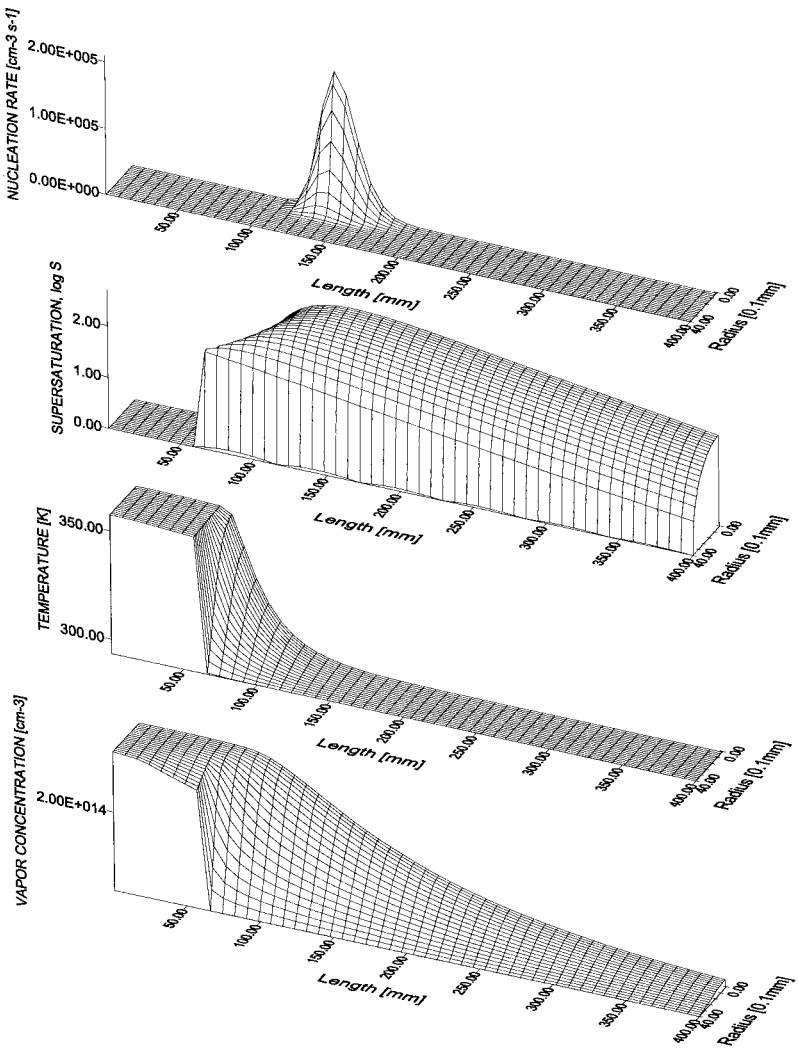

FIG. 6. Results of calculations of temperature, vapor concentration, supersaturation, and nucleation rate distributions inside the internal reactor channel for the system DBP–Ar. The radius of the channel is 4 mm. The length of the channel in this case is 400 mm. The volume flow rate is 5 cm^3/s. Note that the first 60 mm of the channel is part of the saturator section and the remainder is the condenser. Temperature of the saturator is +83.4 °C and temperature of the condenser +20.1 °C. The calculations have been made for the boundary conditions with the gradients described in the text.

In the course of our experimental work, we tried different internal geometries of the saturator at given temperatures of the condenser and saturator and also at a given volume flow rate, and for the given geometry of the condenser. We looked for the highest particle concentration at the outlet of the reactor, measured in all cases by the same TS-3025A counter. Those experiments were made using DBP as a host substance in an argon atmosphere. From these studies, we found the optimal construction of the internal geometry of the saturator that corresponds to the highest detected nucleation rate (see Fig. 2). Again, it should be noted that we cannot define what the true residence time in our saturator is, because these calculations are not so trivial as in the case where the entire internal shape of the saturator, including the outlet, is a tube of constant diameter. Nevertheless, based on the measurements of the nucleation rate dependence on volume flow rate (similar to what was made by Hämeri *et al.*,[17] and Bedanov *et al.*),[3] we believe that the vapor concentration of DBP at the inlet to the channel actually corresponds to the equilibrium vapor pressure of DBP at the saturator temperature. Clearly the direct answer to the residence time question can be only obtained from a direct measurement of the vapor concentration at the outlet of the saturator. We plan to make such measurements in future studies, particularly when we study water vapor nucleation.

2. Temperature measurements

The next important question relates to the correct measurement of the temperature of the reactor, especially in the region of the thermo-insulation between the saturator and the condenser. In order to provide uniform temperature conditions for the entire saturator, as well as for the entire condenser (or at least to diminish the temperature gradients as much as possible), all parts of the reactor (excluding the insulating Teflon® gasket between saturator and condenser) were made from aluminum (Fig. 2). Using thin (0.025 cm diameter) K-type thermocouples, the temperature was measured at different locations inside the aluminum body of both the saturator and the condenser and along the entire internal channel of the reactor as well. We discuss temperature measurements again later.

At a temperature difference of 64.2 °C between the saturator and the condenser bodies (saturator=84.3, condenser =20.1 °C), the temperature at the interface of the internal saturator channel (the face of the cone—see Fig. 2) was less

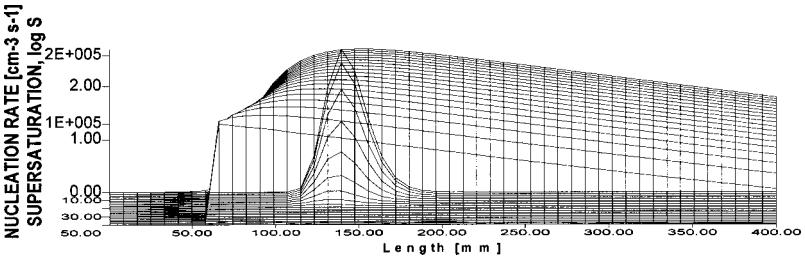

FIG. 7. Supersaturation and nucleation rate profiles, calculated for the same conditions as shown in Fig. 6, are superimposed in order to visually demonstrate that the nucleation rate peak is located in the region where the supersaturation changes very slowly.

than the temperature inside the other internal parts of the saturator by no more than 2 °C. The temperature increases nearly linearly from 83.2 °C (at the interface) up to 84.1 °C during the first 40 mm and then it increases up to 84.3 °C within the next 20 mm. At this point it becomes stable and equal to the temperature of the main part of the aluminum body of the saturator.

For the condenser the total temperature difference between the inside of the internal channel and the whole aluminum body was no more than 0.7 °C (20.8 °C at the cone face, decreasing to 20.1 °C over the first 30 mm of the internal channel, and then remains stable). As already noted above, because of the cone shape of both saturator and condenser faces and the corresponding concave cone shape of the Teflon® gasket (Fig. 2), we have been able to attain a 1 mm thick insulation layer between the internal channels of the saturator and of the condenser.

For such a geometry, it is a good approximation to use a step function to characterize the temperature conditions in the region where the ''hot'' flow leaves the saturator and enters the condenser. We solve the equations of heat and mass transfer using a factorization method and in the numerical calculations, we typically use a 1 mm length step along the axial direction. Thus, the 1 mm insulation thickness ideally represents the boundary conditions used in our calculations. We can also take into account the temperature (and consequently the equilibrium vapor concentration) gradient along the channel walls by incorporating the proper temperature (vapor concentration) into the boundary conditions.

Our calculations show that for a DBP–Ar system, the boundary condition adjustment makes only a very moderate change to the results. In the calculation, we note that the gas diffusion coefficient is typically lower than the thermal diffusivity by about a factor of 5. At a volume flow rate 5 cm^3/s and an internal channel diameter 8 mm, the nucleation rate peak occurs in the vicinity of the central axis at a distance about 10 cm from the beginning of the condenser. As an example, if we put into the boundary conditions all the gradients described above and then compare the results with the calculations made under the assumption that the temperature of the entire saturator is 84.3 °C and the temperature of the entire condenser is 20.1 °C, we obtain the result that the nucleation temperature calculated under the former conditions with gradients is less than that calculated according to the second one by only 0.01 °C. This is certainly within the experimental measurement accuracy. The supersaturation value calculated for the first case is $S=505$ and for the second case $S=520$. Finally, the nucleation rate is $J=100\,000$ and 63 000 particles/cm^3/s, respectively, for cases 1 and 2. The accuracy of the particle concentration measurements (see corresponding topic below) for DBP is about 20%. Thus, while we cannot say that the differences produced by temperature gradients are totally negligible, it appears they are not large. Gradients may become very important for a system like water–helium, because both thermal and gas diffusion coefficients are large and of similar magnitude. We shall present results of calculations for such a system in a separate paper.

3. Computational errors and uncertainties

The next question is about the computational procedure itself. What is the accuracy of the calculations of the temperature, vapor concentration, supersaturation, and nucleation rate profiles inside the internal reactor channel, if the initial and boundary conditions are shown to be valid? This question has been discussed from 1982 (Kostrovskii *et al.*[1]) until the present.[3,17,19] The following equations of heat and mass transfer for steady-state conditions with axial symmetry must be solved:

$$V_{\max}[1-(r/R_0)^2]\partial T/\partial z = \alpha[1/r\ \partial/\partial r(r\partial T/\partial r)+\partial^2 T/\partial z^2], \quad (1)$$

$$V_{\max}[1-(r/R_0)^2]\partial C/\partial z = D[1/r\ \partial/\partial r(r\partial C/\partial r)+\partial^2 C/\partial z^2], \quad (2)$$

where T is the temperature, C is the vapor concentration, r and z are the radial and axial coordinates, R_0 is the radius of the internal channel of the reactor, $V_{\max}$ is the maximum flow velocity, $\alpha=\kappa/c_p\rho$ is the thermal diffusivity (where κ is the thermal conductivity, c_p is the isobaric specific heat, ρ is the gas density), and D is the gas diffusion coefficient.

Normally the following boundary conditions can be used for the temperature:

$T(r,0)=$ temperature of saturator,

$T(R_0,z)=$ temperature of condenser.

For the vapor concentration these conditions then become,

$C(r,0)=$ equilibrium concentration at the saturator temperature,

$C(R_0,z)=$ equilibrium concentration at the condenser temperature.

But, as discussed in the previous topic, the boundary conditions are not so simple, because of the temperature gradients along the channel walls.

As an example, we show the boundary conditions used for the directly measured gradients discussed above.

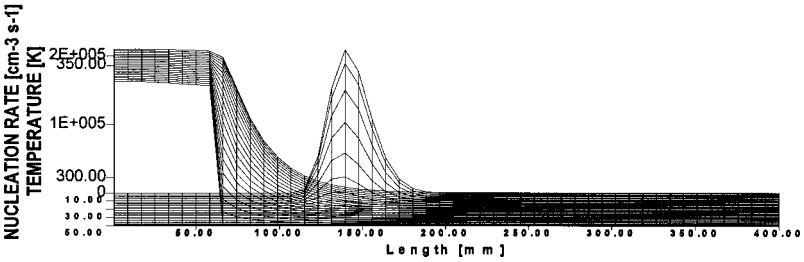

FIG. 8. Temperature and nucleation rate profiles, calculated for the same conditions as shown in Fig. 6, are superimposed to show the temperature drop during the nucleation pulse.

For $Z=0$, $T(r,0)=T_1$,
For $Z=1-20$ mm, $T(R_0,Z)=T_1-0.01Z$,
For $Z=21-60$ mm, $T(R_0,Z)=T(R_0,20)-0.045(Z-20)$,
For $Z=61-90$ mm, $T(R_0,Z)=T_0+0.7-0.023(Z-60)$,
For $Z=91-600$ mm, $T(R_0,Z)=T_0$,

where $T_1=84.3\,^\circ$C is the temperature of the entire body of the saturator and $T_0=20.1\,^\circ$C is the temperature of the entire body of the condenser. The boundary conditions for the vapor concentration also have to be adjusted to represent the equilibrium vapor concentrations corresponding to these new wall temperatures.

Figure 6 shows the results of calculations of temperature, vapor concentration, supersaturation, and nucleation rate for the system DBP–Ar at the temperature of the saturator 83.4 °C and the temperature of the condenser 20.1 °C. Note that the first 60 mm along the *z* axis belongs to the saturator part of the reactor channel; the remainder is the condenser.

Figure 7 shows the nucleation rate [calculated according to the self-consistency correction (SCC) model[25]] and supersaturation profiles, while Fig. 8 shows the nucleation rate and temperature profiles. On inspection of Figs. 7 and 8, we can see that the majority of all the particles (over 80%) nucleate inside a narrow region near the central axis. The diameter and length of the nucleation zone are approximately 2 and 60 mm, respectively. The maximum of nucleation rate is located at about 100 mm from the beginning of the condenser. In this region, the supersaturation *S* varies within the range of 96%–100% of the maximum value of log *S* and the temperature decreases by about 4 °C. By evaluating the maximum of nucleation rate and its location, the corresponding supersaturation and nucleation temperature can be determined. This allows nucleation rate measurements as a function of supersaturation and temperature to be obtained. (For a detailed description of this procedure, the reader is referred to Hämeri *et al.*[17])

The calculations have been made using a computer code and are based on a FORTRAN program first used in 1982[1] for the estimation of nucleation of alcohols. In order to examine how our code performs in comparison with other similar programs, we have made calculations for the same system DBP–nitrogen and for the same initial and boundary conditions used by Bedanov *et al.*[3] The results obtained are practically identical to each other.

As mentioned, our code uses a factorization method. It calculates temperature, vapor pressure, supersaturation, and nucleation rate profiles inside the internal reactor channel. Initial input parameters to the model include measured particle concentration, temperatures of the saturator and of the condenser, length of the channel, number of steps along the channel, number of steps along the radial axis, and volume flow rate. After the model is run for these input values, we can analyze the calculated data to refine more precisely the parameters of the nucleation zone itself. The input parameters for the second part include only the geometrical location of that part of the reactor channel which is of particular interest. Also, the second step provides an option of whether to continue calculations or to stop and to write data files. The program is run on a PC.

The program has the same limitations as other similar codes,[3,17,19] because it does not take into account particle–vapor and particle–particle interactions. But these interactions for the system DBP–argon do not play any important role up to a particle concentration of 100 000 cm^{-3}. With respect to the frequently discussed question of whether or not to take into account the axial dispersion term,[1,19] this program allows a selection of both ways. We performed both tests and found that for DBP–Ar axial dispersion is negligible.

Finally, there are questions about the physicochemical properties of both DBP and Ar that are required for making these calculations. Table I shows the molecular weight, density, equilibrium vapor pressure, surface tension of DBP, density, thermal conductivity, specific heat of Ar at constant pressure, and diffusion coefficient of DBP in Ar. We have used the same vapor pressure data, density, and surface tension for DBP as Bedanov *et al.*[3] and Hämeri *et al.*[17] The thermal diffusivity of argon has been calculated using the handbook[24] data of thermal conductivity, isobaric specific heat, and density. Because we are dealing with a mixture of

TABLE I. Physicochemical properties of DBP and Ar. The parameters are: *M*—molecular weight of dibutylphthalate, ρ_{dbp}—density of DBP, P_e—equilibrium vapor pressure of DBP, σ—surface tension of DBP, ρ_{argon}—density of Ar, κ—thermal conductivity of Ar, C_p—isobaric specific heat of Ar, *D*—diffusion coefficient of DBP in Ar. Temperature is given in K and pressure in Torr (1 Torr=133.322 Pa).

DBP
$M=278.35\ (g/\mathrm{mol})$
$\rho_{dbp}=1.0492-0.000\,67(T-293.15)\pm0.0005(\mathrm{g\ cm^3})$
$\log P_e=7.065-1666/T-547\,700/T^2(\mathrm{Torr})$
$\sigma=0.033\,93-0.000\,089\,4(T-293.15)\pm0.000\,05\ (\mathrm{N/m})$
Ar
$\rho_{argon}=6.9572+-0.036\,853\,9T+8.592\,28E-005T^2+$
$-7.447\,52E-0.08T^3(10^{-3}\ \mathrm{g/cm^3})$
$\kappa=174.45+0.465(T-293.15)(10^{-4}\ \mathrm{W\,m^{-1}\,K^{-1}})$
$C_p=522\ (\mathrm{J\,kg^{-1}\,K^{-1}})$
$D=0.0005T-0.1065\ (\mathrm{cm^2/s})$

TABLE II. Sensitivity analysis of the calculations. The results have been obtained at fixed temperatures of condenser Tc (C) and of saturator Ts (C). Thermal diffusivity as well as diffusion coefficient were varied within ±10%. The changes of nucleation temperature Tn (K), supersaturation S, experimental nucleation rate Je ($cm^{-3}\,s^{-1}$), and theoretical (SCC theory has been used) nucleation rate Jt ($cm^{-3}\,s^{-1}$) are shown.

	Tc	Ts	Tn	log S	log Je	log Jt
Thermal diffusivity used	20.1	84.3	294.28	2.70	4.02	4.84
Thermal diffusivity×0.9	20.1	84.3	294.55	2.66	4.02	4.30
Thermal diffusivity×1.1	20.1	84.3	294.10	2.73	4.02	5.28
Diffusion coefficient used	20.1	84.3	294.28	2.70	4.02	4.84
Diffusion coefficient×0.9	20.1	84.3	294.23	2.74	4.00	5.39
Diffusion coefficient×1.1	20.1	84.3	294.48	2.66	4.06	4.31

argon and DBP, it may lead (according to Hämeri *et al.*[17]) to a change of thermal diffusivity within a range of ±10%. We have performed the same sensitivity analysis as Hämeri *et al.*,[17] i.e., we have made calculations varying the thermal diffusivity within the range of ±10%. The results are presented in Table II. One can see that this variation does not significantly affect the experimental nucleation rate nor the nucleation temperature. It does, however, moderately affect the supersaturation ($\log S$ changes no more than ±2%). Thus, this effect changes the estimated theoretical nucleation rate by less than ±0.5 orders of magnitude or a factor of 3.

Measured data for the gas diffusion coefficient of DBP in argon are not available in the handbook. Hence, in order to obtain it, we have carried out a thorough comparative analysis of available data of diffusion of DBP vapor in nitrogen[3,17] and in air,[24] as well as data for the range of several other substances (e.g., octane), whose diffusion has been measured in different ambient gases (nitrogen, argon, and air).[24] In this way, we believe we can define the limits of possible deviations of the diffusion of DBP–Ar within ±10%. We have performed a sensitivity analysis similar to that performed for thermal diffusivity. The results are also presented in Table II. Again one can see that gas diffusion coefficient deviations have the same influence on the accuracy of the results as shown for thermal diffusivity.

4. Particle concentration measurements

The final question concerns the accuracy of particle concentration measurements. One might think that, with the available commercial ultrafine condensation particle counters (like TSI-3025A), the technique of particle counting in an air flow would be well understood. However, the results obtained during our study indicated that the situation is still not entirely ideal. We have tested the ability of TSI-3025A to measure the concentration of the particles freshly nucleated from water, pentanol, pentadecane, ethylene glycol, glycerin, and DBP over a wide range of nucleation temperatures (from about −30 up to +20 °C). The counter only worked well for DBP over the entire range of temperatures studied. It worked with some restrictions for ethylene glycol and for glycerin, although some problems arose at room temperatures at high concentration levels. It does not work at all for pentanol, pentadecane, and water.

Because this paper focuses on the study of DBP, we do not discuss these problems here in great detail (they will be covered in a separate paper). We note briefly that the most likely source of the problem arises from the capillary tube inside the TSI-3025A (Fig. 9). It appears that ethylene glycol and glycerin particles under certain conditions (particle size and concentration) cannot pass through this capillary. This

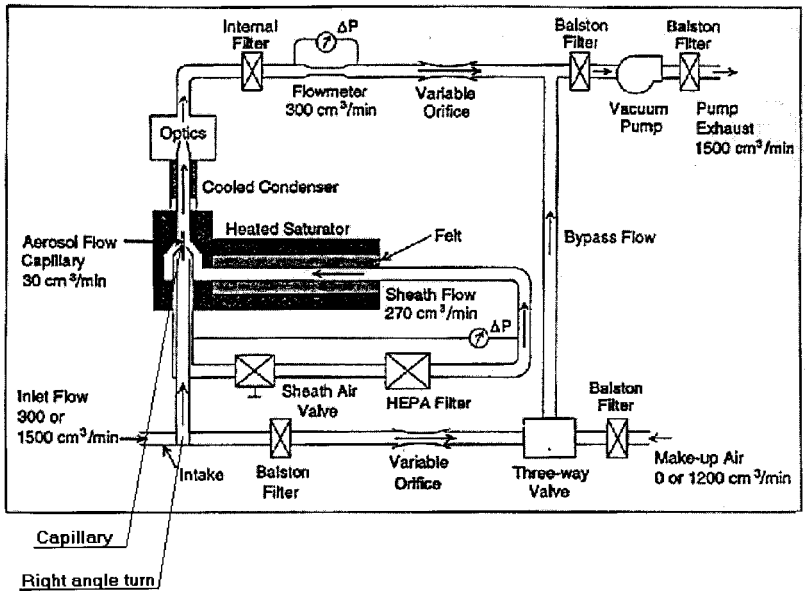

FIG. 9. Schematic of the ultrafine condensation particle counter TSI-3025A. The locations of potential particle loss (capillary and right angle turn) are indicated.

conclusion is based on using a TSI-3010 counter, which does not have this capillary in parallel with the TSI-3025A. It is not entirely clear why we have a problem with water, pentanol, and pentadecane particles. It may be a result of evaporation of the particles, flow impairment in the capillary, interaction (or lack thereof) with the *n* butanol (which is used for the enlargement of the particles injected into the TSI counter), or some other effect.

Some counting discrepancies occur even for DBP particles, indicating possible sampling line losses. We performed measurements with two versions of the TSI-3025A: a standard model with a right angle turn and another, a special model loaned to us by TSI, with a straight tube for delivery of particles to the counting volume. The comparison of DBP particle concentration measurements made by the standard counter and the special model showed that the special counter gave on average 20% higher values than the regular one.

Another possible source of particle counting inaccuracy is the evaporation of the aerosol during its delivery to the counting volume. Because DBP has a sufficiently low vapor pressure, this effect cannot play a role for conditions near room temperature. However, the importance of the evaporation is likely to increase when the condenser temperature is reduced below room temperature. Unfortunately, as a result of the construction and geometry of the TSI-3025A counter, we are not able to provide immediate delivery of freshly formed particles to the counting volume. In that sense, the Vohra–Heist construction[19] provides certain advantages, because the wall of the condenser section is transparent (quartz). On one hand, this construction allows particles to be counted directly in the condenser, but, on the other, it makes it difficult to provide good temperature stability. Ideally, a counting chamber should be placed directly at the outlet of the condenser. We plan to do this in our future work. At the moment we note that our measured nucleation rate at $-21.3\,^{\circ}\mathrm{C}$ lies very close (about a factor of 10 higher) to Bedanov's[3] data (at $-23.5\,^{\circ}\mathrm{C}$) and much higher (several orders of magnitude) than Hämeri's[17] data (at $-22.3\,^{\circ}\mathrm{C}$). It is clear that evaporation will result in a lower nucleation rate. While these comparisons with other data do not provide direct evidence, they at least confirm that evaporative losses are not significant in our case.

C. Summary of errors and uncertainties

In summary, we can say that, at the current state of the development of the laminar flow tube reactor, the uncertainty of the wall temperature measurement is $0.1\,^{\circ}\mathrm{C}$ and its effect on the computed supersaturation is negligible. At present, no technique is available to measure the temperature in the gas accurately without disturbing the flow. However, because the temperature can be measured at any location along the aluminum body of both the saturator and condenser, including the critically important gradients along the walls of the internal channel of the reactor, we can include these gradients into the boundary conditions of the calculations, thus defining the temperature in the reactor channel with as much detail as possible.

There is a possible source of moderate error as a result of the unknown vapor concentration at the beginning of the internal channel. Such an uncertainty can change the initial conditions and may lead to incorrect calculations of the vapor concentration distribution and, consequently, to inaccuracies in defining the supersaturation; although as it has been discussed above, experiments with varying of the flow rate have shown that the initial conditions are correct. However, for full confidence, the vapor concentration at the outlet of the saturator needs to be measured.

Physicochemical parameters used in the calculations may also be questionable, but as shown above those uncertainties lead at most to a $\pm 10\%$ uncertainty in supersaturation. Particle concentration measurements when the condenser is near room temperature should not produce more than a 20% error. Evaluation of evaporative losses of the particles formed at condenser temperatures below room temperatures will be made in future studies.

Generally speaking we note that the entire system is very stable and the results are reproducible. Indeed, measurements presented in this paper were repeated three times over a one-year period using slightly different modifications of the LFTR (mostly these modifications relate to the internal geometry of the saturator and to the interface between the saturator and the condenser). During the measurements, the system operated continuously through an entire day (about 8–10 h without interruption) and the results were still reproducible. Both vertical and horizontal orientations of the LFTR were tried and no difference was observed. Since DBP has a relatively high viscosity, the liquid film formed on the walls of the reactor channel does not affect the nucleation process. Events such as dripping from the reactor walls were observed only rarely and only after about 8 h of continuous operation. In any case this latter kind of disturbance was easily distinguishable from the nucleation process.

III. RESULTS AND DISCUSSION

The experiments were conducted in two modes. First, at a fixed condenser temperature, the saturator temperature was varied. This mode results in a nucleation rate dependence upon supersaturation at a given nucleation temperature (isothermal nucleation rate). This kind of experiment is carried out in discrete steps. Because of the time required to reach temperature equilibrium between the aluminum body of the saturator and the molecular sieves impregnated with DBP, it is not possible to provide correct measurements under continuous change of the saturator temperature. Hence, each measurement is made after a complete temperature equilibrium of the saturator has been achieved. (During some of the controlled measurements, we have allowed a 30–60 min time interval for each experimental point in order to assure that both temperature and particle concentration remained stable during the measurement.) Also, we note that the slope of each experimental curve remains essentially constant (see Fig. 10) over the entire measured particle concentration range (up to 100 000 particles/cm^3 is possible using the TSI-3025A counter). This behavior implies that the measurements of nucleation of DBP vapor presented here are not affected by coagulation processes.

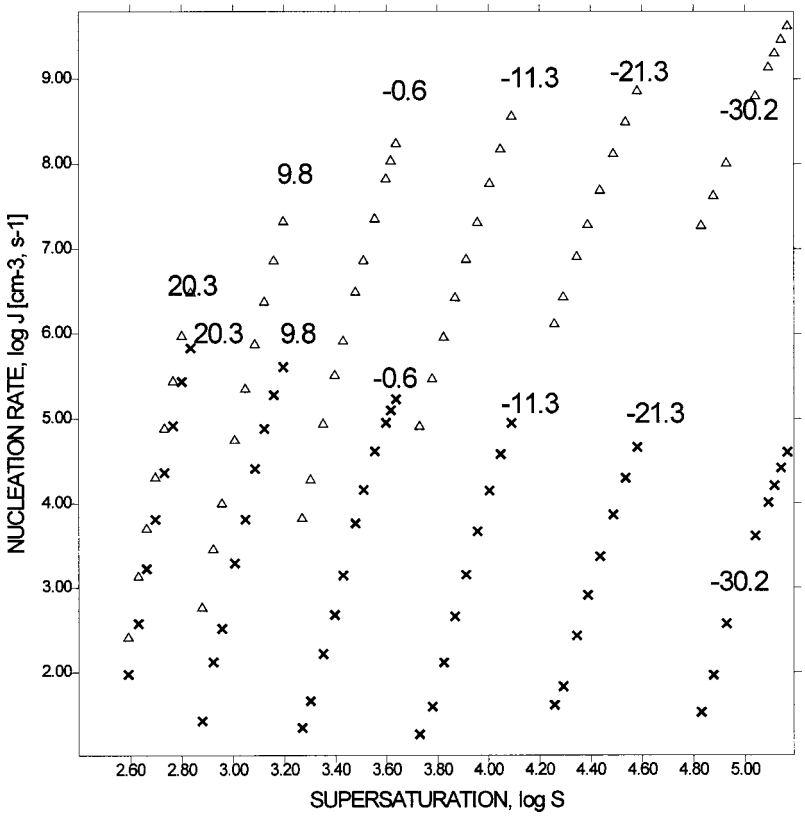

FIG. 10. Nucleation of DBP in Ar. The experimental results (crosses) of nucleation rate J dependence on supersaturation S and theoretical predictions (triangles) made using SCC theory. The nucleation temperatures (C) are indicated at the top of each data set (except for -30.2 °C).

The second mode was carried out at a fixed saturator temperature, while varying the condenser temperature. This mode results in a nucleation rate dependence upon temperature at a given vapor pressure (isobaric nucleation rate). These types of experiments were made because of the particular interest in a recent theoretical breakthrough[5–8] based on the second nucleation theorem, which allows the estimation of important energetic characteristics of the critical cluster. Initially our measurements were carried out in a discrete mode. This type of the experiment, however, does not require establishing temperature equilibrium of the condenser with some foreign substance. We have demonstrated that the results from measurements in the continuous mode do not differ from those obtained in the discrete mode. Subsequently, measurements were made in the continuous mode.

A. Comparison with SCC model of nucleation

Figure 10 shows our experimental data and the comparison with the theoretical predictions based on the SCC theory.[25] Table III gives the numerical values of those data. Two main points can be made. First, the slopes of the experimental curves are consistent with the theoretical predictions. It would therefore appear that the SCC model (and the classical theory on which it is based) can correctly account for the critical cluster size in these experiments. Second, the temperature dependence of nucleation rate does not follow the theoretical predictions. This is in agreement with expectations. In particular, it has been emphasized by McGraw and Laaksonen[4] that a theory based on the classical capillarity approach does not allow prediction of the correct temperature dependence. One can see that the discrepancies with the theoretical predictions increase with decreasing temperature and, therefore, with decreasing critical cluster size. Generally speaking, this conclusion is reasonable, because, as we shall show in the next section, the critical cluster size is only six molecules in size at -30.2 °C. Classical considerations should break down under these conditions.

B. Analysis of data with nucleation theorems

A method has recently been developed for the extraction of information about the energetics of critical clusters from experimental data on the nucleation rate. The critical cluster is the size that is equally likely to grow or to decay under the conditions prevailing in the supersaturated vapor; it is regarded as the principal intermediate state in a droplet nucleation event. The analysis uses the two nucleation theorems,[1–7,26] which are general results based on the thermodynamics of cluster formation.

The main result of this analysis is a plot of the excess internal energy of a critical cluster against its size in molecules. The excess internal energy is the difference between the energy of the cluster, and the corresponding energy the component molecules would possess if they were part of a bulk condensed phase under the same conditions; it is loosely related to the surface energy.

The two nucleation theorems are

$$\left(\frac{\partial \ln J}{\partial \ln S}\right)_T = 1 + i^* \tag{3}$$

and

$$\left(\frac{\partial \ln J}{\partial T}\right)_S = (L - kT + E_x(i^*))/kT^2, \tag{4}$$

TABLE III. Experimental results and comparison with the predictions of SCC (self-consistency correction) nucleation theory. Six sets of the experimental points have been obtained at six fixed temperatures of condenser Tc (C). Saturator temperature Ts (C) has been varied. Nucleation temperature Tn (K), supersaturation S, experimental nucleation rate Je ($cm^{-3}\,s^{-1}$), and theoretical nucleation rate Jt ($cm^{-3}\,s^{-1}$) are presented.

Tc	*Ts*	*Tn*	log *S*	log *Je*	log *Jt*	*Tc*	*Ts*	*Tn*	log *S*	log *Je*	log *Jt*
−30.3	38.4	242.98	4.857	1.527	7.486	−1.3	61	272.46	3.24	1.04	3.42
−30.3	39.3	242.98	4.904	1.963	7.834	−1.3	62.2	272.48	3.291	1.34	4.12
−30.3	40.3	242.98	4.955	2.572	8.209	−1.3	63	272.48	3.324	1.6611	4.57
−30.3	42.5	242.99	5.066	3.611	8.985	−1.3	64.2	272.5	3.374	2.21	5.21
−30.3	43.5	242.99	5.115	4.006	9.32	−1.3	65.3	272.51	3.419	2.67	5.77
−30.3	44	242.99	5.14	4.208	9.483	−1.3	66.1	272.52	3.451	3.14	6.169
−30.3	44.5	242.99	5.165	4.418	9.644	−1.3	67.3	272.53	3.499	3.7608	6.736
−30.3	45	242.99	5.189	4.603	9.802	−1.3	68.1	272.54	3.531	4.15	7.1
						−1.3	69.2	272.55	3.575	4.61	7.583
−21.6	45	251.8	4.283	1.61	6.35	−1.3	70.3	272.56	3.618	4.94	8.04
−21.6	45.7	251.8	4.317	1.83	6.663	−1.3	70.8	272.56	3.638	5.09	8.25
−21.6	46.8	251.81	4.37	2.43	7.13	−1.3	71.3	272.57	3.657	5.22	8.45
−21.6	47.7	251.81	4.41	2.9	7.5						
−21.6	48.7	251.81	4.46	3.36	7.89	8.9	71.2	282.88	2.9	1.42	3.09
−21.6	49.8	251.82	4.51	3.86	8.32	8.9	72.3	282.9	2.942	2.12	3.77
−21.6	50.8	251.82	4.55	4.29	8.68	8.9	73.3	282.91	2.976	2.51	4.3
−21.6	51.8	251.82	4.6	4.66	9.046	8.9	74.5	282.93	3.026	3.288	5.03
						8.9	75.6	282.94	3.0673	3.8	5.62
−11.8	51.7	261.81	3.69	1.02	4.55	8.9	76.6	282.96	3.104	4.4	6.13
−11.8	52.9	261.82	3.753	1.26	5.178	8.9	77.6	282.97	3.14	4.87	6.63
−11.8	54	261.83	3.8	1.59	5.72	8.9	78.6	282.98	3.177	5.27	7.1
−11.8	55	261.84	3.84	2.11	6.2	8.9	79.6	283	3.214	5.6	7.56
−11.8	56	261.85	3.89	2.656	6.665						
−11.8	57	261.85	3.93	3.15	7.1	19.1	81.7	293.37	2.611	1.97	2.75
−11.8	58	261.86	3.979	3.66	7.53	19.1	82.8	293.4	2.65	2.57	3.46
−11.8	59.1	261.87	4.026	4.14	7.98	19.1	83.7	293.41	2.681	3.22	4.02
−11.8	60.1	261.88	4.069	4.579	8.379	19.1	84.7	293.43	2.716	3.81	4.61
−11.8	61.1	261.88	4.112	4.94	8.7608	19.1	85.7	293.45	2.75	4.36	5.178
						19.1	86.7	293.47	2.784	4.91	5.721
						19.1	87.7	293.49	2.818	5.43	6.243
						19.1	88.7	293.51	2.852	5.82	6.744

where J is the rate of formation of critical clusters, S is the supersaturation ratio, T is the temperature, i^* is the number of molecules in a critical cluster, $E_x(i^*)$ is its excess internal energy, k is Boltzmann's constant, and L is the latent heat of condensation per molecule. The nucleation theorems in this form assume that the vapor phase can be described as an ideal gas. Corrections for nonideal effects have recently been derived[8] but quantifying them requires knowledge of the second virial coefficient. Approximate calculations on *n*-pentanol,[8] together with physical considerations, suggest that they should be small, so we neglect the corrections.

The nucleation theorems enable us to calculate the size and excess energy of a critical cluster, if we know the dependence of the nucleation rate on temperature and supersaturation. We therefore need to fit a function $J(S,T)$ to the experimental data. We use a fitting function of the form

$$\ln J = a - b(c/T-1)^3/(\ln S)^2, \tag{5}$$

where a, b, and c are fitting parameters. This function is similar to the phenomenological expression which Hale[27,28] showed to be effective in correlating nucleation rates for a variety of substances. It is consistent with the following expression for the excess energy:

$$E_x(i^*) = \frac{3b^{1/3}ck}{2^{2/3}}(1+i^*)^{2/3} - L + kT. \tag{6}$$

The latent heat of condensation per molecule, L, can be calculated from the empirical expression for the saturation vapor pressure P_e as a function of temperature, given in Table I, through use of the Clausius–Clapeyron equation $d\ln P_e/dT = L/(kT^2)$. Hence L/k (in units of K^{-1}) is given by

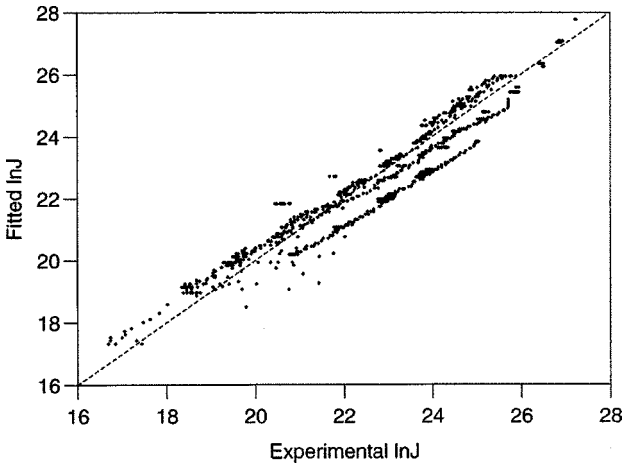

FIG. 11. Evaluation of the success of the fitting function. The dots display the experimental and fitted values of $\ln J$. The dashed line represents a perfect fit to the data.

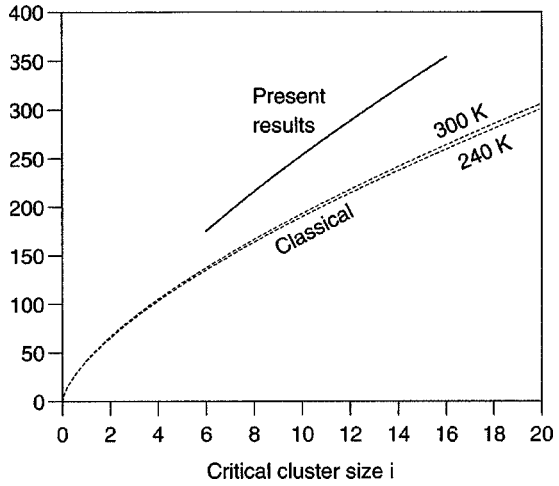

FIG. 12. The excess energy as a function of critical cluster size, expressed in units of kT_0, where $T_0=273.15$ K. Solid line: calculations from the experimental data, valid within the range of S, T values covered in the experiments. Dashed lines: predictions of classical nucleation theory.

$$L=3836k+2\,522\,000k/T. \tag{7}$$

Fitting a function of the form of Eq. (5) to experimental data from the present investigation produced $a=67.4$, $b=5730$, and $c=490$ K. Figure 11 demonstrates that the function describes the data well. The graph of $E_x(i^*)$ against i^* (in units of kT_0, where $T_0=273.15$ K) is plotted in Fig. 12. Also shown, for comparison, are the predictions of classical nucleation theory, which are given by

$$E^*_{xcl}=kT^2\left(\frac{1}{2\sigma}\frac{d\sigma}{dT}-\frac{(36\pi)^{1/3}}{3}\left(\frac{3}{\sigma}\frac{d\sigma}{dT}-\frac{2}{\rho_{dbp}}\frac{d\rho_{dbp}}{dT}-\frac{3}{T}\right)\frac{\sigma}{kT\rho_{dbp}^{2/3}}i^{*2/3}\right), \tag{8}$$

where E^*_{xcl} represents the classical excess energy evaluated at the classical critical size i^*_{cl}. Here, ρ_{dbp} is the liquid molecular density, and σ is the surface tension. We use physical properties given in Table I.

The critical clusters investigated here are remarkably small, containing as few as six molecules, and there is no reason to expect them to be described by classical nucleation theory. It is instructive to compare the results depicted in Fig. 12 with calculations using the latent heat and the number of dangling (unsatisfied) bonds in a cluster. The latent heat per molecule at 273.15 K, from Eq. (7), is $L=47.8\,kT_0$. Now, a molecule in the bulk liquid will interact with around 12 nearest neighbors, if the arrangement bears any resemblance to that in a close-packed solid. If we associate the latent heat of condensation with the formation of nearest-neighbor bonds, then each bond will therefore contribute a binding energy of around $L/6$. An isolated cluster of six molecules, arranged as a compact fragment of a close-packed structure, is sketched in Fig. 13. It possesses 12 bonds in all, so that the total energy is about $-12L/6$. According to this simple model, the excess energy for the 6-cluster will therefore be $-12L/6-6(-L)=4L=191\,kT_0$. Similarly, a cluster of 15 molecules, arranged as the close-packed fragment sketched in Fig. 13, would contain 42 bonds, and the excess energy would be $-42L/6-15(-L)=8L=383\,kT_0$. These estimates are just a little higher than the values indicated in Fig. 12. The cluster energies we extract from the nucleation data are therefore not unrealistic, and would be ideal for testing more detailed models of the binding of DBP clusters.

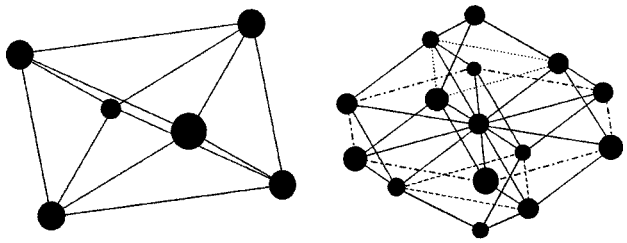

FIG. 13. Suggested structures of molecular clusters of 6 and 15 molecules. Both are fragments of close-packed structures. (111) planes in the 15-cluster are indicated in different line styles to make the structure easier to recognize.

C. Comparison with other experimental data

Figures 14–16 allow comparison of our experimental results with previously measured data.[3,18,20] Comparison with data obtained by two other experimental groups[3,18] shows that in one case (Bedanov *et al.*[3]) there is agreement at low temperature (around -20 °C), but discrepancies grow with increasing temperature. Quite the opposite is seen with the Hämeri *et al.*[18] data, which are in agreement at room temperature, but then as the temperature decreases, the discrepancy grows very quickly until it reaches an enormous value (approximately seven orders of magnitude) at a temperature of -27 °C.

Clearly, such a large discrepancy cannot be caused by any of the possible reasons discussed earlier. In particular, because we have used practically the same physicochemical data (with the exception of a different carrier gas), the calculations themselves can not be the source of the discrepancy. We are inclined to assume that it is most likely the temperature measurements that may be the cause of these drastic differences. Perhaps use of a relatively large diameter (0.5 mm) thermocouple is not appropriate. During our measurements, we have tested three types of thermocouples: 0.025, 0.25, and 0.5 mm in diameter. The thinnest one is too sensitive and it is practically impossible to use for gas temperature measurements. A comparison between the second and third types has shown a difference that increases below room temperature. The thickest (0.5 mm) thermocouple may indicate a temperature up to several degrees warmer than the 0.25 mm one in the region -20 to -30 °C, depending on how deep the thickest thermocouple is slipped into the thermo-well. For this reason, all our measurements were made using the 0.25 mm type. We also suspect that the deviations with our own earlier measurements[16] may have been caused by the same reason, since a 0.5 mm thick thermocouple was used in the earlier work.

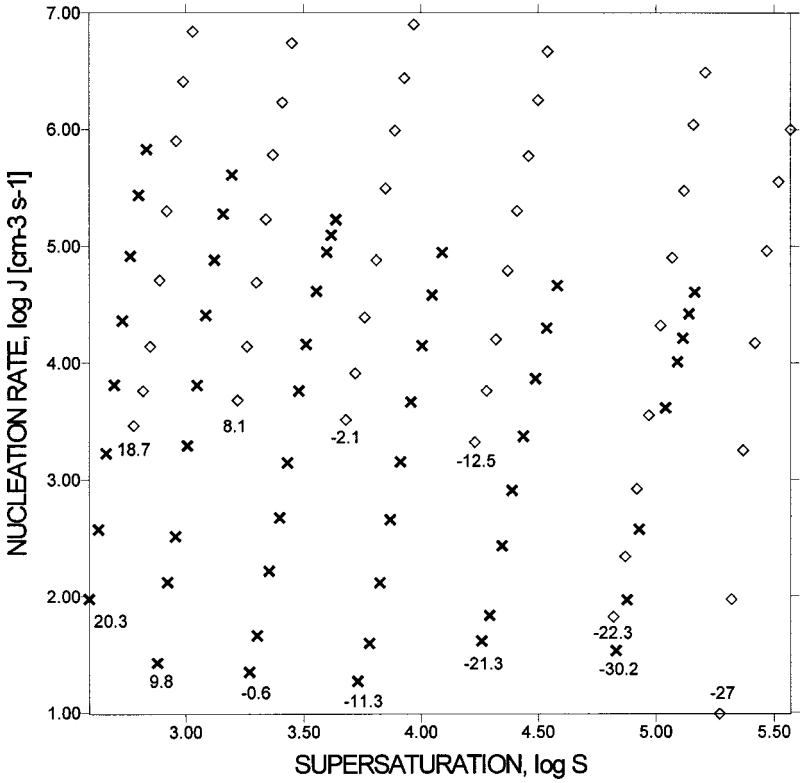

FIG. 14. Nucleation of DBP in Ar. The nucleation rate J dependence on supersaturation S. Comparison of our current experimental data (crosses) and the Hämeri *et al.* (Ref. 15) results (diamonds). The nucleation temperatures (C) are indicated at the lowest point of each data set.

IV. CONCLUSIONS AND FUTURE PLANS

We have clearly shown that the laminar flow tube reactor technique can be used as a quantitative tool for nucleation measurements. There is still some work that needs to be done to evaluate possible sources of uncertainties, such as vapor concentration at the inlet to the internal channel of the reactor and evaporative losses of particles formed at conditions below room temperature. Also, careful attention needs to be paid to the choice of physicochemical parameters used in calculations.

The data gathered have provided significant insight into the properties of small molecular clusters of DBP. Through

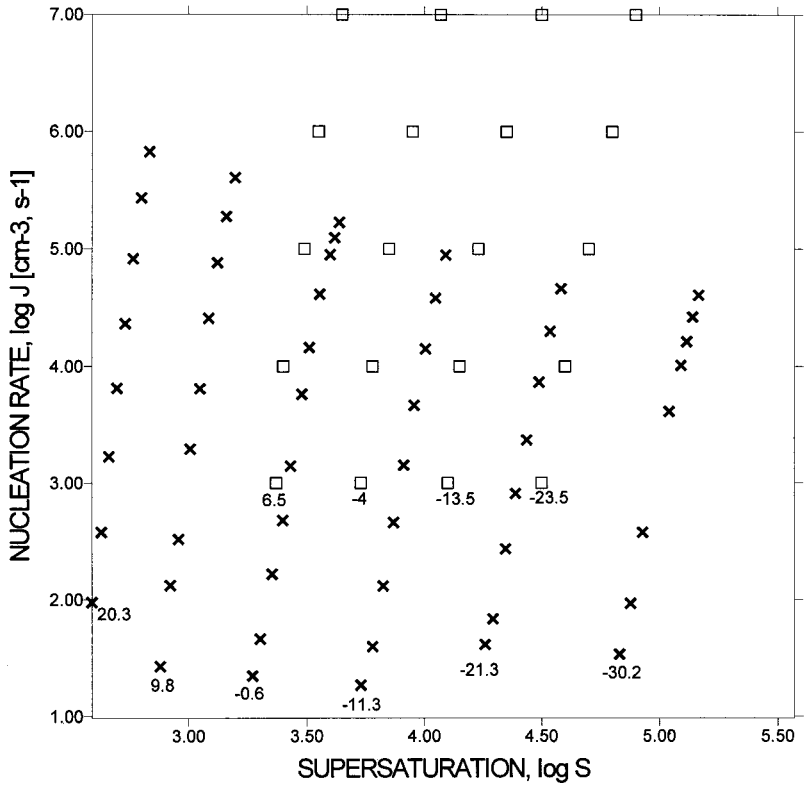

FIG. 15. Nucleation of DBP in Ar. The nucleation rate J dependence on supersaturation S. Comparison of our current experimental data (crosses) and the Bedanov *et al.* (Ref. 3) results (squares). The nucleation temperatures (C) are indicated at the lowest point of each data set.

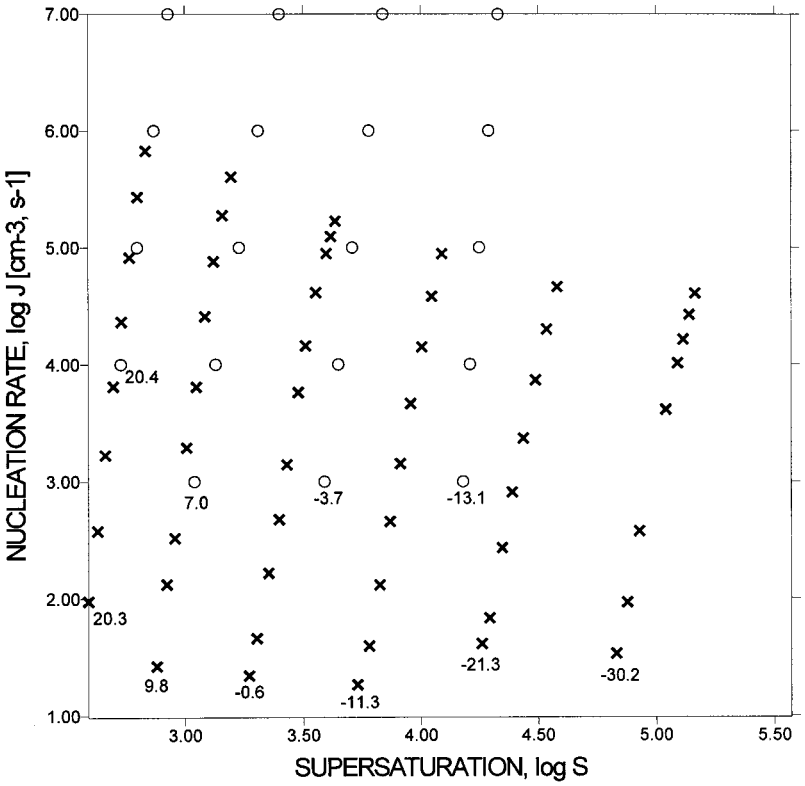

FIG. 16. Nucleation of DBP in Ar. The nucleation rate J dependence on supersaturation S. Comparison of our current experimental data (crosses) and our previous results (Ref. 17) (circles). The nucleation temperatures (C) are indicated at the lowest point of each data set.

use of the nucleation theorems, the dependence of the nucleation rate on temperature and supersaturation has yielded the excess energies of clusters consisting of as few as six molecules. We have shown that these results are not consistent with the capillarity approximation, which is to be expected. However, if we model the clusters are fragments of a close-packed structure, and estimate the excess energies on the basis of the number of broken surface bonds and the measured latent heat of condensation, then we find good agreement. It suggests that more detailed molecular modeling would be profitable.

We note that this study has been made using the very convenient working substance DBP, for which the Lewis number ($\mathrm{Le}=\alpha/D$) is typically much larger than unity for any of the carrier gases used (for argon Le is approximately equal to 5). Our next studies will include such substances as glycerol, ethylene glycol, range of alkanes, a range of alcohols, and water. For some of them, like light alkanes, light alcohols, and particularly for water, it is not so easy to find appropriate conditions, where thermal processes prevail in comparison with diffusion. However, some preliminary work has already been done and the results will be published in future papers.

ACKNOWLEDGMENTS

This work has been supported by the Atmospheric Chemistry Program of the U.S. Department of Energy (DOE) under Contract No. DE-AC06-76RLO 1830. Pacific Northwest National Laboratory is operated for DOE by Battelle Memorial Institute. We would also like to express great appreciation to TSI staff Stan Kaufman, Nathan Birkeland, and Maynard Havlicek for their support in dealing with questions on CPC applications and limitations. Discussions with Gennady Kodenyov were always very fruitful. And Vitaly Kostrovskii, who together with Gennady Kodenyov in the mid 1970s was the first inspirer of the development of the LFTR technique, is kindly acknowledged. Michael Knott is supported by the U.K. Engineering and Physical Science Research Council.

[1] V. G. Kostrovskii, V. B. Mikheev, and M. S. Shtein, Kolloidn. Zh. **44**, 773 (1982).
[2] D. Kashchiev, J. Chem. Phys. **76**, 5098 (1982).
[3] V. M. Bedanov, V. S. Vaganov, G. V. Gadiyak, G. G. Kodenyov, and E. A. Rubakhin, Khim. Fiz. **7**, 555 (1988).
[4] R. McGraw and A. Laaksonen, Phys. Rev. Lett. **76**, 2754 (1996).
[5] Y. Viisanen, R. Strey, and H. Reiss, J. Chem. Phys. **99**, 4680 (1993).
[6] I. J. Ford, J. Chem. Phys. **105**, 8324 (1996).
[7] I. J. Ford, Phys. Rev. E **56**, 5615 (1997).
[8] M. Knott, H. Vehkamäki, and I. J. Ford, J. Chem. Phys. **112**, 5393 (2000).
[9] V. B. Mikheev and V. G. Kostrovskii, Kolloidn. Zh. **53**, 653 (1991).
[10] R. H. Heist and H. He, J. Phys. Chem. Ref. Data **23**, 781 (1994).
[11] P. E. Wagner and R. J. Strey, J. Phys. Chem. **85**, 2694 (1981).
[12] R. Strey, P. E. Wagner, and Y. Viisanen, J. Chem. Phys. **98**, 7748 (1994).
[13] J. L. Katz, J. Chem. Phys. **52**, 4733 (1970).
[14] R. H. Heist and H. Reiss, J. Chem. Phys. **59**, 665 (1973).
[15] F. Peters, Lect. Notes Phys. **309**, 535 (1988).
[16] C. C. Luijten, C. C. M. , P. Peeters, and M. E. H. van Dongen, J. Chem. Phys. **109**, 3553 (1999).
[17] K. Hämeri, M. Kulmala, E. Krissenel', and G. Kodenyov, J. Chem. Phys. **105**, 7683 (1996).
[18] K. Hämeri and M. Kulmala, J. Chem. Phys. **105**, 7696 (1996).
[19] V. Vohra and R. H. Heist, J. Chem. Phys. **104**, 382 (1996).
[20] V. B. Mikheev and N. S. Laulainen, J. Aerosol Sci. **28**, Suppl. 1, S167 (1997).
[21] H. V. Nguyen, K. Okuyama, T. Mimura, Y. Kousaka, R. C. Flagan, and J. H. Seinfeld, J. Colloid Interface Sci. **119**, 491 (1987).
[22] J. C. Barrett and T. J. Baldwin, J. Aerosol Sci. **31**, 633 (2000).

[23] M. Wilck, K. Hameri, F. Stratmann, and M. Kulmala, J. Aerosol Sci. **29**, 899 (1998).
[24] N. B. Vargaftic, *Handbook on Thermophysical Properties of Gases and Liquids* (Fizmatgiz, Moscow, 1963).
[25] M. Blander and J. L. Katz, J. Stat. Phys. **4**, 55 (1972).
[26] D. W. Oxtoby and D. Kashchiev, J. Chem. Phys. **100**, 7665 (1994).
[27] B. N. Hale, Phys. Rev. A **33**, 4156 (1986).
[28] B. N. Hale, Metall. Trans. A **23**, 1863 (1992).